Two-Color Resonant Four-Wave Mixing: A Tool for Double Resonance Spectroscopy

Eric A. Rohlfing, Joseph D. Tobiason, and James R. Dunlop

Combustion Research Facility
Sandia National Laboratories
Livermore, CA 94551

Skip Williams

Division of Chemical Science and Technology
Los Alamos National Laboratory
MS J586
Los Alamos, NM 87545

ABSTRACT

Two-color resonant four-wave mixing (RFWM) shows great promise in a variety of double-resonance applications in molecular spectroscopy and chemical dynamics. One such application is stimulated emission pumping (SEP), which is a powerful method of characterizing ground-state potential energy surfaces in regions of chemical interest. We use time-independent, diagrammatic perturbation theory to identify the resonant terms in the third-order nonlinear susceptibility for each possible scheme by which two-color RFWM can be used for double-resonance spectroscopy. After a spherical tensor analysis we arrive at a signal expression for two-color RFWM that separates the molecular properties from purely laboratory-frame factors. In addition, the spectral response for tuning the DUMP laser in RFWM-SEP is found to be a simple Lorentzian in free-jet experiments. We demonstrate the utility of RFWM-SEP and test our theoretical predictions in experiments on jet-cooled transient molecules. In experiments on C_3 we compare the two possible RFWM-SEP processes and show that one is particularly well-suited to the common situation in which the PUMP transition is strong but the DUMP transitions are weak. We obtain RFWM-SEP spectra of the formyl radical, HCO, that probe quasibound vibrational resonances lying above the low threshold for dissociation to H+CO. Varying the polarization of the input beams or PUMP rotational branch produces dramatic effects in the relative intensities of rotational lines in the RFWM-SEP spectra of HCO; these effects are well-described by our theoretical analysis. Finally, RFWM-SEP spectra of HCO resonances that are homogeneously broadened by dissociation confirm the predicted lineshape and give widths that are in good agreement with those determined via unsaturated fluorescence depletion SEP.

1. INTRODUCTION

Resonant four-wave mixing (RFWM) is a nonlinear optical technique that has been demonstrated as a spectroscopic and remote sensing technique for stable molecules and transient species in a variety of gas phase environments. Degenerate four-wave mixing (DFWM), in which all of the fields are of a single frequency that is resonant with a molecular transition, has been used as a diagnostic in combustion[1-6] and reacting plasmas.[7-9] In addition, DFWM has been employed as a method of detecting transitions in stimulated emission pumping (SEP) spectroscopy.[10,11] Two-color RFWM, by which we mean that there are two input frequencies in resonance with two distinct molecular transitions, has also been used for double resonance spectroscopy (PUMP and PROBE) of stable molecules[12,13] and for background-free SEP spectroscopy of stable[14] and transient species.[15]

Signal generation in RFWM is often viewed as the formation of and diffraction from laser-induced population gratings.[16] The conceptually appealing grating picture is particularly applicable to two-color RFWM in which there is a distinct difference in frequency (and possibly temporal delay) between the two grating forming beams and the probe beam. Thus two-color techniques have also become known as laser-induced grating spectroscopy (LIGS). We have used two-color LIGS to examine nonfluorescent molecules in free jets, namely predissociating NO_2[17] and azulene undergoing internal conversion in its first excited singlet state.[18] The induced-grating picture can also be used to

DISCLAIMER

Portions of this document may be illegible in electronic image products. Images are produced from the best available original document.

explain saturation phenomena via the production of anharmonic gratings.[18] Finally, probing the temporal evolution of the induced grating enables one to perform transient grating experiments, which are a staple of ultrafast laser experiments in gas and condensed phases.[16] We have developed a photofragment transient grating technique and have used it to determine the velocity distributions of very slow NO fragments produced in the near-threshold photolysis of jet-cooled NO_2.[19]

We have recently presented a detailed theoretical and experimental investigation of two-color RFWM applied to SEP spectroscopy.[20] The theoretical objective of that work was to describe the two-color RFWM process in a formalism more amenable to molecular spectroscopy than the laser-induced grating picture. Our approach, which was an extension of the recent work by Williams, Zare, and Rahn on DFWM,[21] combined time-independent diagrammatic perturbation theory[22-25] with spherical tensor analysis[26] to derive a general signal expression for RFWM that accounts for polarization and relaxation effects in the weak-field limit. The power of this approach lies in the complete separation of molecular properties from factors that describe the interaction of the electric fields in the laboratory frame. Furthermore, we evaluated the RFWM-SEP lineshape functions for tuning the DUMP laser for the specialized case of free-jet expansions, in which residual Doppler broadening is neglected and no collisional relaxation occurs. In this article we shall provide a brief review of the experimental and theoretical results for RFWM-SEP presented in Ref. 20 and provide additional generalization of the theoretical approach to other two-color RFWM schemes applicable to different double-resonance spectroscopies.
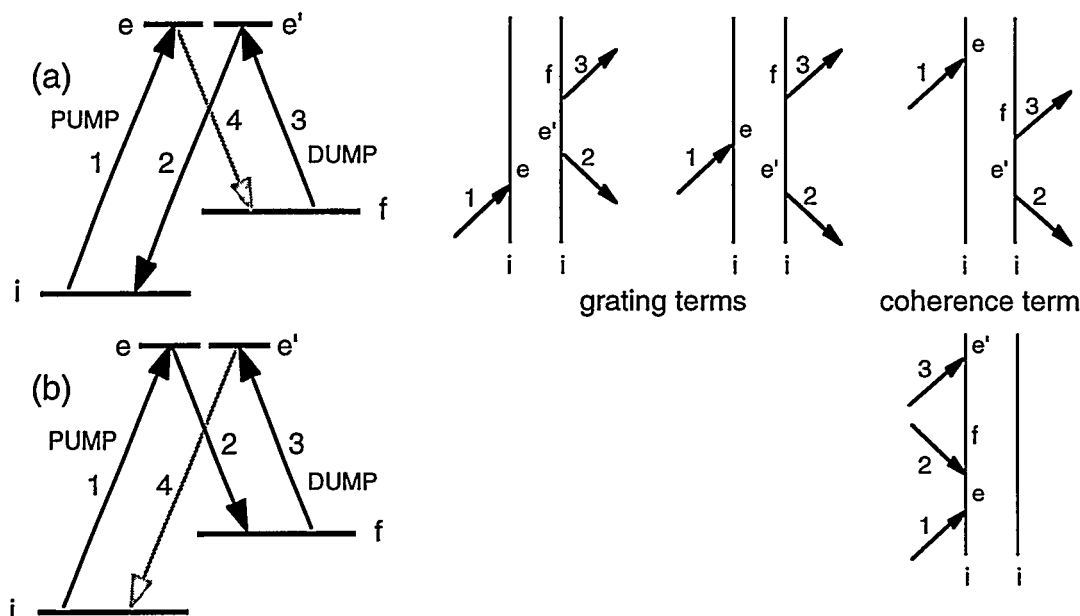

Fig. 1 Folded energy-level schematics and double-sided Feynman diagrams used to identify the resonant terms in $\chi^{(3)}$ for two-color RFWM appropriate to SEP spectroscopy: **(a)** $\omega_1=\omega_2$ (PUMP) and $\omega_3=\omega_4$ (DUMP); **(b)** $\omega_1=\omega_4$ (PUMP) and $\omega_2=\omega_3$ (DUMP).

2. TWO-COLOR RFWM SIGNAL EXPRESSION

In Figs. 1-3 we present the three-level energy diagrams and beam (field) labelling for every possible application of two-color RFWM to double resonance spectroscopy. The level labels correspond to individual magnetic sublevels of each rovibronic state; i denotes levels in the initially populated ground state and e and f denote levels in the initially unpopulated excited states. (The primed and unprimed letters denote degenerate magnetic sublevels, either the same or different, of a particular level.) Figures 1 and 2 each illustrate double resonances in which level e is in common. The folded diagram in Fig. 1 corresponds to SEP in which with the e-i transition is the PUMP and the e-f transition is the DUMP; Fig. 2 shows the unfolded version in which the f-e transition is more typically called the PROBE. For each of the excited-state common schemes there are two possible RFWM processes: (a) $\omega_1=\omega_2$ (PUMP) and $\omega_3=\omega_4$ (DUMP

or PROBE) and (b) $\omega_1=\omega_4$ (PUMP) and $\omega_2=\omega_3$ (DUMP or PROBE). Figure 3 illustrates a double resonance in which the ground-state level i is in common; here the transitions are now e-i (PUMP) and f-i (PROBE). There is only one unique RFWM process for this scheme since the interchange of labels e and f (i.e., PUMP and PROBE transitions) does not alter $\chi^{(3)}$.
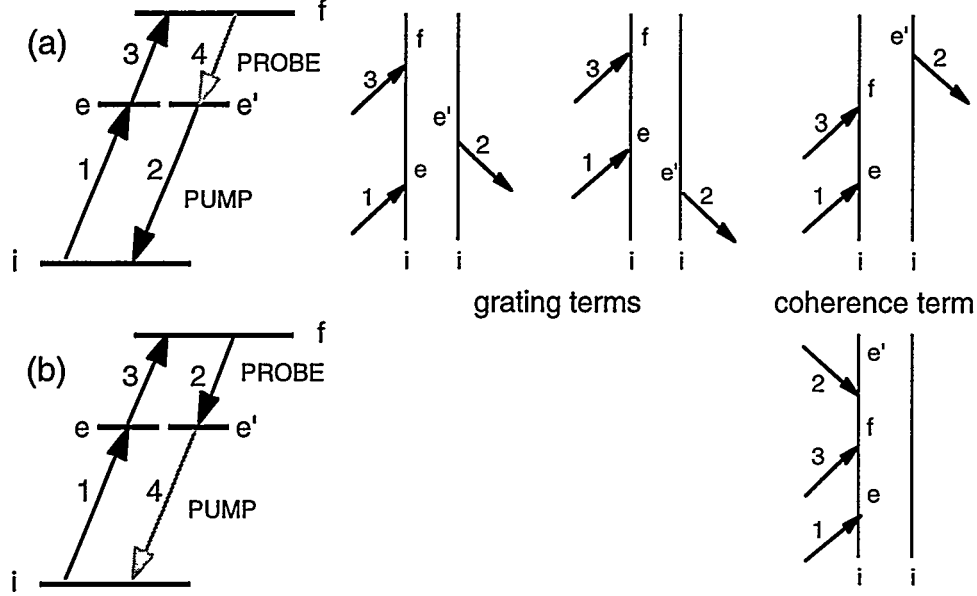

Fig. 2 Unfolded energy-level schematics and double-sided Feynman diagrams used to identify the resonant terms in $\chi^{(3)}$ for two-color RFWM appropriate to double-resonance spectroscopy via the excited state: **(a)** $\omega_1=\omega_2$ (PUMP) and $\omega_3=\omega_4$ (PROBE); **(b)** $\omega_1=\omega_4$ (PUMP) and $\omega_2=\omega_3$ (PROBE).

In four-wave mixing three incoming waves with electric fields $E_1(r,t)$, $E_2(r,t)$, and $E_3(r,t)$, propagation vectors k_1, k_2, and k_3, unit polarization vectors ε_1, ε_2, and ε_3, and frequencies ω_1, ω_2, and ω_3 interact through the third-order nonlinear susceptibility $\chi^{(3)}$ to generate a fourth field, E_4, with propagation vector k_4, polarization ε_4, and frequency ω_4. The RFWM signal intensity is proportional $\left|\chi^{(3)}\right|^2$. The general perturbation expression for $\chi^{(3)}$ for four-wave mixing consists of 48 terms that completely describe the interaction of the electric fields with the molecular system.[22-24] These terms differ in the time ordering of the interaction fields and in the permutations of the quantum states involved. Evaluating all of these terms is a formidable task in general; however, in RFWM the intensity at a particular resonance in the spectrum is dominated by only a few terms. These terms are represented for each two-color RFWM process in Figs. 1-3 using double-sided Feynman diagrams. For example, the three diagrams for the RFWM-SEP process in Fig. 1(a) correspond to the three possible time orderings of the input fields (time increases from bottom to top of the diagram) and yield the following expression for $\chi^{(3)}$ in the perturbative (weak-field) limit

$$\chi^{(3)}_{RFWM}(-\omega_4,\omega_1,\omega_3,-\omega_2) =$$

$$\frac{N}{6\varepsilon_0\hbar^3}\left\{\sum_{all\,M}\frac{\rho_{ii}^{(0)}\langle e|\varepsilon_1\cdot\mu|i\rangle\langle i|\varepsilon_2^*\cdot\mu|e'\rangle\langle e'|\varepsilon_3\cdot\mu|f\rangle\langle f|\varepsilon_4^*\cdot\mu|e\rangle}{\left(\Delta_P+k_1\cdot v-i\Gamma_{ei}\right)\left[(k_1-k_2)\cdot v-i\Gamma_{ee'}\right]\left(\Delta_D+k_4\cdot v-i\Gamma_{ef}\right)}\right.$$

$$-\sum_{all\,M}\frac{\rho_{ii}^{(0)}\langle e|\varepsilon_1\cdot\mu|i\rangle\langle i|\varepsilon_2^*\cdot\mu|e'\rangle\langle e'|\varepsilon_3\cdot\mu|f\rangle\langle f|\varepsilon_4^*\cdot\mu|e\rangle}{\left(\Delta_P+k_2\cdot v+i\Gamma_{e'i}\right)\left[(k_1-k_2)\cdot v-i\Gamma_{ee'}\right]\left(\Delta_D+k_4\cdot v-i\Gamma_{ef}\right)}$$

$$\left.-\sum_{all\,M}\frac{\rho_{ii}^{(0)}\langle f|\varepsilon_4^*\cdot\mu|e\rangle\langle e|\varepsilon_1\cdot\mu|i\rangle\langle i|\varepsilon_2^*\cdot\mu|e'\rangle\langle e'|\varepsilon_3\cdot\mu|f\rangle}{\left(\Delta_P+k_2\cdot v+i\Gamma_{e'i}\right)\left[\Delta_D-\Delta_P+(k_3-k_2)\cdot v-i\Gamma_{fi}\right]\left(\Delta_D+k_4\cdot v-i\Gamma_{ef}\right)}\right\}. \tag{1}$$

We define the spectral detunings for the PUMP and DUMP transitions respectively as

$$\Delta_P = \frac{\left(E_e - E_i\right)}{\hbar} - \omega_1 \qquad \text{and} \qquad \Delta_D = \frac{\left(E_e - E_f\right)}{\hbar} - \omega_3, \qquad (2)$$

where E_n is the energy of the level n. The relaxation and dephasing rates Γ_{nm} are defined as

$$\Gamma_{nm} = \frac{\left(\Gamma_n + \Gamma_m\right)}{2} + \Gamma_{nm}^{pd}, \qquad (3)$$

where $\Gamma_n = 1/\tau_n$, with τ_n being the lifetime of the level n, and where Γ_{nm}^{pd} is the pure collisional dephasing rate of the dipolar coherence between the levels n and m. Expressions similar to Eqs.(1)-(3), with the appropriate label changes and definitions of spectral detunings, are readily obtained for the other two-color RFWM processes from the diagrams in Figs. 1-3.

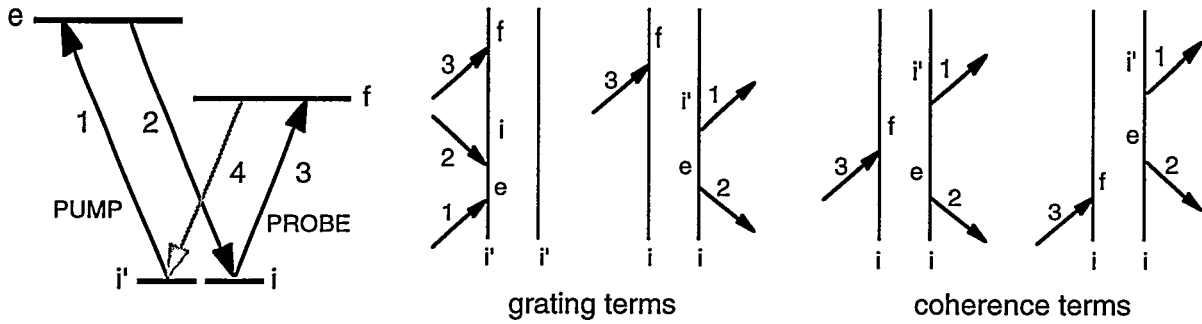grating terms   coherence terms

Fig. 3 Energy-level schematics and double-sided Feynman diagrams used to identify the resonant terms in $\chi^{(3)}$ for two-color RFWM appropriate to double-resonance spectroscopy via the ground state.

The RFWM processes in Figs. 1(a) and 2(a) are often referred to as excited-state LIGS since the first two diagrams (and the first two terms in Eq. (1)) can be interpreted·in terms of formation and diffraction from an excited-state population grating (although orientation and alignment gratings may contribute as well). The two-photon decay rate for these terms, $\Gamma_{ee'} = \Gamma_e = 1/\tau_e$, represents the lifetime of the excited state. Thermal motion in the sample also contributes to the decay of the excited-state grating. However, when the PUMP and DUMP (or PROBE) laser pulses overlap in time the last diagram in Figs. 1(a) and 2(a) also contributes to the signal. This term may be thought of as a coherence between levels i and f that decays with the characteristic two-photon relaxation rate Γ_{fi}. The RFWM processes shown in Figs. 1(b) and 2(b) are completely described by this type of coherence. The RFWM process in Fig. 3 is also often referred to as ground-state LIGS and the first two diagrams in Fig. 3 do represent ground-state gratings. However, when both PUMP and PROBE pulses overlap in time there are two additional coherence terms (this time between levels e and f) that contribute to the RFWM signal. There are four terms (diagrams) in Fig. 3 because both PUMP and PROBE transitions sample the initially populated level and thus any of the three input fields may interact first. By contrast, in the excited-state common schemes in Figs. 1 and 2 only the PUMP transition samples the initially populated state and field 3, which is always resonant with the DUMP or PROBE transition, cannot interact first.

The development of the perturbative expression for $\chi^{(3)}$ (Eq. 1) into a general RFWM signal equation separates into the analysis of the numerators, which contain the four transition moments summed over all possible magnetic sublevels, and the resonant denominators, which contain the spectral response and can be removed from the summations because the dipolar dephasing rates are indpendent of M. The M-level sums may be re-ordered so that for each two-color RFWM process the numerators reduce to a four-photon matrix element, which, for the schemes in Figs. 1 and 2 is

$$\rho_{ii}^{(0)} \sum_{M_e} \langle e|(\varepsilon_1 \cdot \mu_1)(\varepsilon_2^* \cdot \mu_2)(\varepsilon_3 \cdot \mu_3)(\varepsilon_4^* \cdot \mu_4)|e \rangle, \tag{4}$$

where the transition dipoles are subscripted for bookeeping in a spherical tensor analysis.[20] This analysis is developed fully in Ref. 20 for RFWM-SEP and in Ref. 21 for DFWM and will not be described in detail here. This method provides a well developed and efficient way of using the inherent symmetry of the system and allows the separation of the molecular properties from purely geometric factors.[26] The final result is a general signal expression that is valid in the weak-field limit, which for the RFWM-SEP schemes in Fig. 1is

$$I_{RFWM} \propto [N_i]^2 \left[B_{ie}(J_i, J_e)\right]^2 \left[B_{ef}(J_e, J_f)\right]^2 I_1 I_2 I_3 \left|\pounds(\Delta_P, \Delta_D)\right|^2 \left[G_F^T(\varepsilon_4, \varepsilon_1, \varepsilon_3, \varepsilon_2; J_i, J_e, J_f)\right]^2. \tag{5}$$

In Eq. (5) N_i is the total population of the level i in the absence of applied fields, $B_{ie}(J_i, J_e)$ and $B_{ef}(J_e, J_f)$ are the Einstein coefficients for the PUMP and DUMP transitions, respectively, $I_1 I_2 I_3$ is the product of the three input intensities, $\left|\pounds(\Delta_P, \Delta_D)\right|^2$ is the total lineshape function, and $G_F^T(\varepsilon_4, \varepsilon_1, \varepsilon_3, \varepsilon_2; J_i, J_e, J_f)$ is a total geometric factor that depends solely on the polarization unit vectors of the electric fields ε_j and the total angular momentum quantum numbers J_i, J_e, and J_f. The spectroscopic and dynamic properties of interest are contained in the Einstein coefficients and the lineshape function. The Einstein coefficients describe the strength of the interaction of the molecule with the excitation fields in the molecular frame and can be related to other, well-cataloged molecular parameters such as the absorption cross-section, oscillator strength, linestrength, spontaneous emission lifetime, and transition-dipole moment. The lineshape function depends on the inhomogeneous broadening due to the molecular velocity distribution and on homogeneous broadening, due either to collisions or intramolecular nonradiatve processes (i.e., predissociation, internal conversion, etc.). As shown in Ref. 20, the lineshape function for tuning the DUMP laser is a simple Lorentzian in the collisionless environment of a free jet. The geometric factors are just real numbers that account for the geometry of the interaction of the molecule with the electric fields in the laboratory frame. Simple analytic expressions for $G_F^T(\varepsilon_4, \varepsilon_1, \varepsilon_3, \varepsilon_2; J_i, J_e, J_f)$ are given in Tables I-III of Ref. 20 for the allowed polarization configurations of linearly polarized light in the forward-box phase matching geometry for RFWM-SEP. There are four polarization configurations, denoted YYYY, YXYX, YYXX and YXXY (the field ordering is $\varepsilon_4, \varepsilon_1, \varepsilon_3, \varepsilon_2$) that yield different geometric factors (interchanging X for Y has no effect). For each polarization configuration there are nine possible PUMP/DUMP rotational branch combinations, i.e., there are nine possible paths denoted by $J_i \to J_e \to J_f$. Hence there are a total of 36 geometric factors tabulated in Ref. 20. The geometric factors for the two processes given in Fig. 1(a) and (b) are related by the simple interchange of fields 2 and 4, i.e., $\varepsilon_4, \varepsilon_1, \varepsilon_3, \varepsilon_2 \leftrightarrow \varepsilon_2, \varepsilon_1, \varepsilon_3, \varepsilon_4$.

Equation (5) can be applied, with minor changes, to each of the other two-color RFWM processes shown in Figs. 2 and 3. For the excited-state processes in Fig. 2 the Einstein coefficients and geometric factors are identical to those for RFWM-SEP. Also, the two processes in Fig. 2(a) and (b) are related by the field interchange, 2↔4. For the ground-state process in Fig. 3 $B_{ef}(J_e, J_f)$ in Eq. (5) must be replaced by $B_{if}(J_i, J_f)$. The geometric factors for the ground-state process are related to those for RFWM-SEP simply by interchanging J_i and J_e in the tables of Ref. 20. (Strictly speaking, one must also perform two field interchanges, 1↔2 and 3↔4, but this has no effect on the geometric factors.) The free-jet lineshape function for the excited-state processes in Fig. 2 is basically identical to that for RFWM-SEP,[20] except that it must be altered to reflect the fact that the two-photon resonance is at the sum of the PUMP and PROBE frequencies, not at their difference. The free-jet lineshape for tuning the PROBE laser is a simple Lorentzian as for RFWM-SEP. The lineshape function for the ground-state process can be evaluated from the resonant denominators contained in the diagrams of Fig. 3.

3. EXPERIMENTAL TECHNIQUE

We perform RFWM-SEP experiments on two transient molecules, C_3 and HCO, that are entrained in a helium free-jet expansion following a piezoelectrically acutated pulsed valve. The carbon trimer, C_3, is generated by the laser vaporization (532 nm) of graphite into the helium flow within a channel prior to the expansion. In this case, the expansion eminates from the 2.5-mm diameter channel following the vaporization region. The formyl radical, HCO, is

generated by the excimer-laser photolysis at 308 nm of acetaldehyde, which is seeded at a concentration of 5% into helium at a total pressure of 1-2 atm and expanded through a 1 or 2 mm-diameter orifice. The photolysis beam (pulse energy 40-60 mJ) is focussed with a 500-mm focal length lens and crosses the expansion 2-5 mm downstream from the orifice.

The PUMP and DUMP frequencies in these experiments are generated from a pair of Nd:YAG-pumped dye laser systems (Continuum NY81C/ Lumonics HD500 and Continuum NY61/ Lumonics HD300). The dye lasers are standard multimode pulsed lasers with nominal pulse widths of 6-7 ns and fundamental linewidths of 0.05-0.10 cm^{-1}. For the C_3 experiments, the PUMP laser excites rotational lines in the $\tilde{A} \, ^1\Pi_u$ - $\tilde{X} \, ^1\Sigma_g^+$ origin band at 405 nm; this wavelength is generated by mixing the dye laser fundamental at 654 nm with the residual Nd:YAG fundamental. The DUMP laser is tuned over the 483-505 nm range to access bending levels with two quanta of antisymmetric stretch in the ground state. For the HCO experiments, the PUMP excites lines in the $\tilde{B} \, ^2A'$- $\tilde{X} \, ^2A'$ origin band at 258 nm; this wavelength is generated from the frequency doubled output of the dye laser. To access the C-O stretch/bend levels in the ground state the DUMP laser, another frequency-doubled dye laser, is tuned over the 318-337 nm region.

Our implementation of RFWM-SEP is nearly identical to that described in our previous work on two-color LIGS.[17] We use the forward box geometry for processes (a) and (b) shown in Fig. 1, where the three input beams, which lie on the corners of a rectangle, propogate in the same direction. The typical half-angle of crossing for the two identical frequency beams (ω_1 and ω_2 for (a) or ω_2 and ω_3 for (b)) is less than 1 degree and the angle of the third beam is chosen to satisfy phase matching conditions.[17] The two identical frequency beams cross in a plane perpendicular to the jet axis, which means that the fringes of their induced population grating (for process (a)) run parallel to the jet axis. This orientation produces long-lived gratings since washout occurs only due to residual transverse velocity in the jet.[17,19]

The interaction region for the RFWM-SEP is typically 10-20 mm downstream of the expansion orifice. In this region LIF excitation spectra of the transient molecules reveal that they are rotationally cooled to 5-15 K. The beam diameter of each of the three input beams is 1-2 mm in the interaction region. In order to compensate for signal beam walk caused by phase matching constraints,[15,17] the signal beam passes through a 1-m-focal-length lens that images the interaction region. The signal beam is then spatially filtered with a short-focal-length lens/pinhole combination, frequency filtered with a bandpass filter to eliminate scattered light at the other input frequency, and detected with a photomultiplier tube. For crossed polarization configurations the input beam polarizations are rotated with double Fresnel rhombs. The input beam at the same frequency as the signal beam has its polarization purified by passage through a Wollaston polarizer. No special polarization purification is applied to the other two input beams. The signal beam, which is produced in a pure linear polarization state, passes through a Glan-Taylor polarizer that is crossed with respect to the Wollaston polarizer.

We obtain FD-SEP spectra of HCO using counterpropogating, identically polarized PUMP and DUMP beams. The HCO fluorescence is collected at right angles to the jet and the laser beams, imaged onto the entrance slit of a 0.75-m monochromator, and detected with a photomultiplier tube. Shot-to-shot fluctuations in the PUMP laser-induced fluorescence are compensated for using the dual-gate normalization scheme employed previously in our FD-SEP studies of jet-cooled species.[27] For HCO, the DUMP pulse is temporally delayed by approximately 50 ns from the PUMP pulse and the depleted fluorescence signal is normalized by a reference fluorescence signal taken prior to the DUMP laser firing.

4. RFWM-SEP RESULTS and DISCUSSION

It is quite common in SEP for the PUMP transition to be significantly stronger than the DUMP transitions of interest, which often have poor Franck-Condon factors from the excited state. One of the great attributes of FD-SEP is that very weak DUMP transitions can often be easily observed simply by increasing the intensity of the DUMP laser. In our applications of RFWM-SEP to transient molecules in free jets, it is not always possible to observe weak DUMP transitions using process (a). The weak-field signal expression, Eq.(5), shows why. The signal varies as the square of the Einstein coefficient, alternatively the cross section, for the DUMP transition. This dependence, coupled with the low number density in the jet and its quadratic effect on the signal, generally reduces the signal level below the background due to scattered light from DUMP beam 3. Simply increasing the DUMP intensity will never cause the
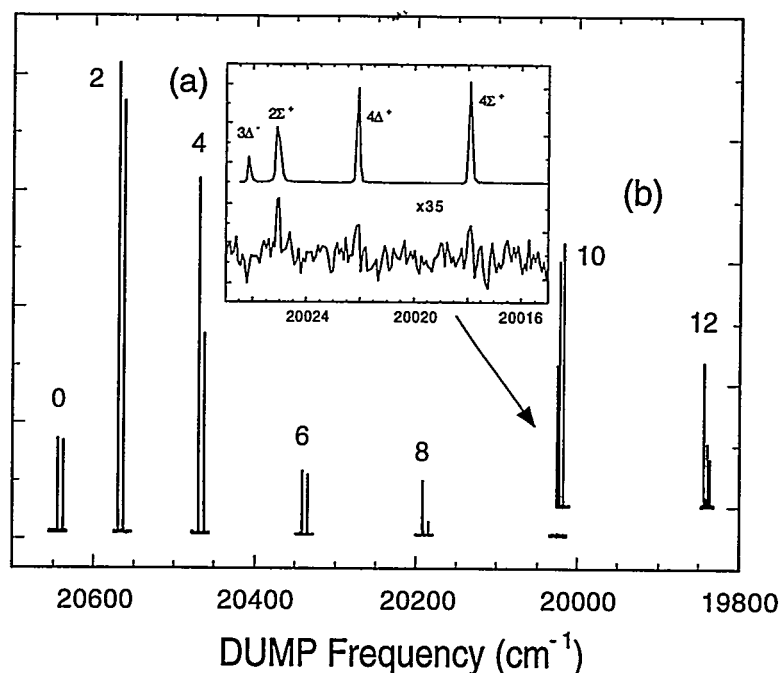
Fig. 4 A comparison of RFWM-SEP spectra (YYYY) of jet-cooled C_3 taken by PUMPing the R(2) line of the A-X origin band. The DUMP reaches levels in the (0,v_2,2) progression, where the linear bending quantum number, v_2, is indicated. **(a)** Spectra obtained using the process in Fig. 1(a) and **(b)** spectra obtained using the process in Fig. 1(b). The insert compares the rotational structure of the (0,10,2) band.

signal to exceed the background because both signal and background increase linearly with DUMP intensity. The scattered light background in process (a) can be reduced by using polarization configurations in which the signal beam is cross polarized to beam 3 (i.e., YYXX and YXXY; see following). However, the scattered light from beam 3 comes primarily from the vacuum chamber windows and its polarization is less than 100% pure. We typically observe a 30-50 fold reduction in scattered light in the cross polarized configurations. RFWM-SEP process (b) offers a much more general solution to this problem because the signal beam is now detected at the PUMP frequency and scattered light from the DUMP beams can be reduced by many orders of magnitude by appropriate frequency filtering. Polarization configurations for process (b) in which the signal beam is cross polarized to beam 1 (YXYX and YXXY) may also be employed to further reduce the scattered light background.

The $\tilde{A}\ ^1\Pi_u$ - $\tilde{X}\ ^1\Sigma_g^+$ cometary band system of C_3 provides an excellent proving ground for RFWM-SEP applications.[20] In Fig. 4 we compare RFWM-SEP survey spectra of the bending progression with two quanta of antisymmetric stretch obtained using the two processes in the YYYY configuration under nearly identical conditions (except for DUMP intensity). The vibrational band strengths in the 0,v_2,2 progression decrease monotonically from a peak at v_2=2.[20] The observed RFWM signals for (a) follow this trend until the signal becomes comparable to the scattered light background at the 0,10,2 level. The insert of Fig. 4 displays an expanded view of this region; note that zero on the left ordinate corresponds to a zero-signal level taken with the detector blocked. Using process (b), with the DUMP intensity increased some 50 fold, we obtain RFWM-SEP spectra of the 0,10,2 band and even weaker features, such as the 0,12,2 band, with an excellent signal-to-background ratio. In fact, we have used RFWM-SEP process (b) to obtain spectra of the much weaker 0,v_2,4 progression with a similar signal-to-background ratio.

The two different RFWM-SEP processes thus provide the experimentalist with tools that should be adequate to observe both strong and weak DUMP transitions. While the choice of which approach to use depends on several factors, a general rule for low-density environments (such as jets) is to detect the signal on the strongest transition since the intensity of the single input beam at that frequency, and the scattered light background due to it, can be minimized. Thus, as illustrated above for C_3, when the PUMP transition is strong, process (b) works well because the intensity of

PUMP beam 1 is kept low and the intensities in the DUMP beams (2 and 3) can be increased in order to bring out weak features. Conversely, in the case of a weak PUMP transition but strong DUMP bands (for example, HCO, see below), process (a) is preferable. The rule of detecting the signal on the stronger of the two transitions is also applicable to the other two-color RFWM processes shown in Figs. 2 and 3.

Our second application of RFWM-SEP is to the $\tilde{B}\,^2A'$- $\tilde{X}\,^2A'$ system of the formyl radical, HCO. This system is ideal for the characterization of quasibound vibrational resonances that lie above the anomalously small threshold to dissociation to H+CO ($\sim$5000 cm^{-1}).[28] The width of a resonance gives its dissociation rate, which is highly mode specific. We use the notation v_1,v_2,v_3 to label the normal modes of HCO, which are the C-H stretch, C-O stretch, and bend, respectively, and use standard asymmetric top rotational notation, $N_{K_aK_c}$, for the rotational levels. The spin-rotation interaction produces states with total angular momentum (neglecting hyperfine interaction) of $J=N\pm1/2$; in most cases this splitting is unresolved. RFWM-SEP process (a) is the appropriate choice for the $\tilde{B}$-$\tilde{X}$ system of HCO since the DUMP transitions are generally much stronger than the PUMP transition.

In Fig. 5 (left) we display RFWM-SEP spectra (using process (a)) of the 0,4,0 resonance of HCO obtained for an R PUMP transition using the YYYY, YYXX, and YXXY polarization configurations. The a-type PUMP transition is $2_{02}\leftarrow1_{01}$, from which we observe DUMP transitions to the 1_{01} and 3_{03} levels (R and P a-type) and the 1_{11}, 2_{11}, and 3_{13} levels (R, Q, and P b-type). Our practical motivation for employing polarization configurations in which the signal is cross polarized to DUMP beam 3 is evident in Fig. 5. The background in the YYYY spectrum represents scattered light that is greatly reduced in YYXX and YXXY. The effect of polarization configuration on the relative rotational line intensities is dramatic and is due entirely to changes in the RFWM geometric factors.

We calculate the relative line intensites for the three spectra in Fig. 5 using the signal expression in Eq. (5) with the geometric factors in Ref. 20. The other input to this calculation are the relative rotational linestrengths, or Hönl-London factors, which enter through $\left[B_{ef}(J_e,J_f)\right]^2$ in Eq. (5). We calculate these using standard spectroscopic approaches with the rotation and spin-rotation constants for the $\tilde{B}$-$\tilde{X}$ origin band.[20] In Fig. 5 (right) we compare the
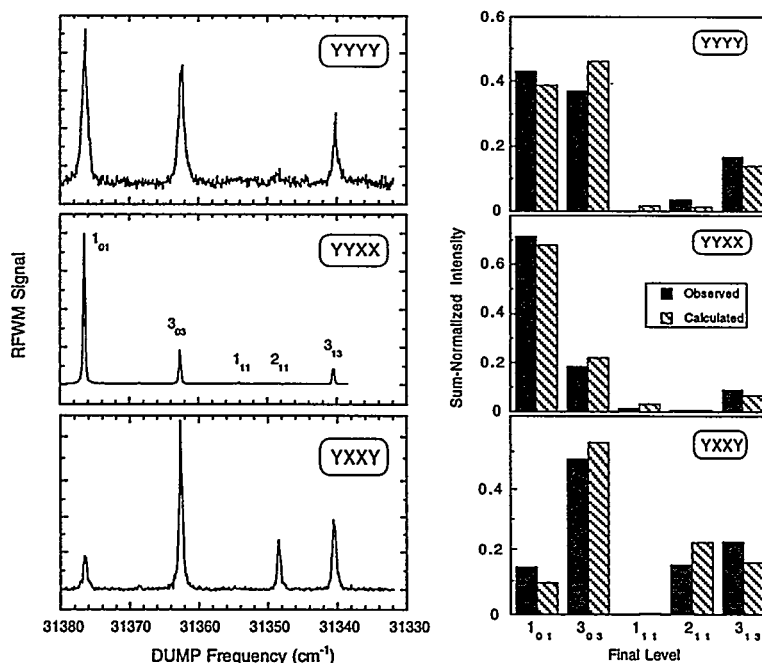

Fig. 5 Left: RFWM-SEP spectra of the (0,4,0) resonance of jet-cooled HCO taken via the origin band of the B-X system using the process in Fig. 1(a) in three different linear polarization configurations ($\varepsilon_4\varepsilon_1\varepsilon_3\varepsilon_2$). The PUMP transition is 2_{02}-1_{01} and the rotational levels accessed by the DUMP are indicated. **Right:** Comparison of observed and calculated relative intensities, normalized by the sum of all lines in the band.

observed and calculated intensities, normalized to the sum of all lines in the band, for the three polarization configurations. The agreement is quite good, with the calculation correctly reproducing the large variations in the relative intensities of RR and RP combinations due to changes in the polarization configuration. Equation (5) also predicts the relative intensities of the rotational lines observed in other RFWM-SEP spectra of HCO.[20] In particular, the geometric factors in Ref. 20 correctly account for the dramatic changes in intensities with polarization configuration and branch type of the PUMP transition.

The homogenous linewidth of an individual DUMP line is of particular interest in HCO because it provides a direct measure of the dissociation rate from the final resonance state. In Fig. 6, we display RFWM-SEP spectra that terminate on the 1_{01} (unresolved spin doublet) of the 0,5,0 and 0,4,1 resonances. As predicted, a simple Lorentzian function accurately represents the observed lineshape for the RFWM-SEP data; fits and residuals are shown in Fig. 6. To verify that the full widths determined from RFWM-SEP spectra agree with those obtained using the more conventional FD-SEP technique, we have obtained FD-SEP spectra of the same lines. These are shown, with Lorentzian fits and residuals, in the lower panels of Fig. 6.
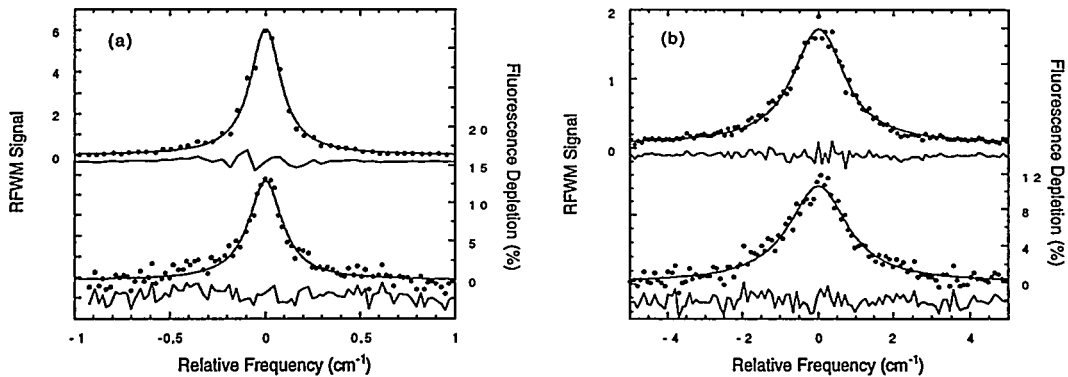

Fig. 6 Comparison of lineshapes for RFWM-SEP (top) and FD-SEP (bottom) spectra of jet-cooled HCO taken via the origin band of the B-X system using the process in Fig. 1(a) in the YYXX configuration. The PUMP and DUMP transitions are both 2_{02}-1_{01}. (a) The (0,5,0) resonance; Γ=0.20(1) cm^{-1}; (b) the (0,4,1) resonance; Γ=1.7(1) cm^{-1}. Lorentzian fits to the spectra are shown; residuals are offset for clarity.

One must be cautious in using FD-SEP to determine widths because of saturation broadening of the DUMP transitions. Note that the depletions shown in Fig. 6 are fairly small; typically we find that the depletion must be less than about 15% in order for the line to be free from saturation broadening. At these small depletions the uncertainty in the fitted widths for FD-SEP are large, 10-20%, and arise almost entirely from fluctuations in the baseline. By contrast, RFWM-SEP spectra typically have negligible baseline noise but do exhibit signal fluctuations that can be quite large. Put another way, the signal-to-background ratio is high in RFWM-SEP but the signal-to-noise ratio at line center may be low. For FD-SEP both ratios are usually identical and are dominated by fluctuations in the fluorescence induced by the PUMP laser. As the signal expression in Eq. (5) shows, noise in the RFWM signal stems from the cubic dependence on input-beam intensities and the quadratic dependence on number density. Shot-to-shot normalization by the laser intensities can be used to reduce the intensity-dependent noise. In these experiments, however, the dominant source of noise in the RFWM signal is the shot-to-shot variation in the HCO number density, for which there is no obvious normalization scheme. Finally, the RFWM-SEP spectra displayed in Fig. 6 are free from saturation effects since they are obtained with far less intensity in the DUMP beam than is typically used for FD-SEP. For example, we do not observe FD-SEP spectra using the DUMP intensities employed in RFWM-SEP and thus the

population depletion of the excited state must be less than 1-2%, which is a typical fluctuation in the normalized fluorescence in our experiments.

In HCO, the homogeneous width and hence the dissociation rate, depends dramatically on the vibrational character of the final resonance state.[28] The pure C-O stretch resonance (0,5,0) exhibits a width that is essentially limited by the laser bandwidth, which is approximately 0.2 cm^{-1} for the frequency doubled dye laser used for the DUMP. The influence of the finite bandwidth and multimode nature of the PUMP and DUMP lasers is not accounted for in our weak-field signal expressions for RFWM-SEP. However, the data in Fig. 6 (a) indicate that the laser-limited lineshape for RFWM-SEP does not deviate substantially from a simple Lorentzian and that the widths in both the RFWM-SEP and FD-SEP spectra are in good agreement. In contrast to the 0,5,0 resonance, the C-O stretch-bend resonance (0,4,1) has a significantly faster dissociation rate as manifested by the significantly larger widths in the SEP spectra in Fig. 6 (b). These widths, 1.67(10) cm^{-1} and 1.86(20) cm^{-1} for the RFWM-SEP and FD-SEP spectra, respectively, are significantly greater than the laser bandwidth. Thus the comparison of the 0,4,1 spectra provides a more stringent test of the equivalence of homogeneous widths using the two techniques since any effects of finite laser bandwidth are negligible. We therefore conclude that we can accurately determine resonance widths (or dissociation rates) from the RFWM-SEP spectra of HCO in cases where the width is not significantly laser limited.

5. CONCLUSIONS

Two-color RFWM has the potential to become another powerful tool for double-resonance molecular spectroscopy, as we have demonstrated here and elsewhere[20] for SEP. The prime advantage of RFWM approaches over linear techniques is in the generation of a background-free, coherent signal beam. Sensitivity is the major limitation of two-color RFWM, since the signal scales quadratically with number density, PUMP cross section, and DUMP (PROBE) cross section (see Eq. (5)). We have presented (Figs. 1-3) the energy-level/beam schemes and double-sided Feynman diagrams, which identify the resonant terms in $\chi^{(3)}$, for all possible applications of two-color RFWM to double-resonance spectroscopy. The weak-field signal expression for RFWM-SEP that results from a spherical tensor analysis[20] may be generalized to the other processes depicted in Figs. 2 and 3. In particular, the geometric factors derived in Ref. 20 are applicable (with minor notation changes) in all cases.

In our RFWM-SEP experiments on C_3 and HCO, we have demonstrated the applicability of RFWM-SEP to jet-cooled transient molecules and illustrated the practical advantage of the process in Fig. 1(b) in probing very weak DUMP transitions. One can generalize this result to create a practical guideline for any two-color RFWM process: the signal field should be resonant with the stronger of the two transitions. This arrangement, which can be augmented by a crossed polarization configuration, insures the minimization of scattered light background. The general signal expression in Eq. (5) accurately describes the effect of polarization configuration and PUMP branch type on the relative intensities observed in the RFWM-SEP spectra of HCO. In particular, these experiments demonstrate the validity of the geometric factors since these are the **only** terms in Eq. (5) through which changes in polarization configuration or PUMP transition affect the relative intensities in a given DUMP spectrum. Finally, the lineshape function for tuning the DUMP laser in RFWM-SEP has been confirmed to be a simple Lorentzian and the full widths obtained from RFWM-SEP spectra of HCO are in excellent agreement with those derived from unsaturated FD-SEP spectra. This agreement holds both for transitions with laser-limited widths and for those in which the homogeneous width due to dissociation of the resonant level is significantly larger than the laser bandwidth.

The use of polarization configurations has great potential in two-color RFWM. As we have demonstrated, the configurations in which the signal beam is cross polarized to the input beam of the same frequency provide the practical advantage of greatly reducing the scattered light background. In collisional environments these configurations have the added advantage of eliminating signal contributions from thermal gratings, which can often dominate the resonant signal of interest.[6,13] Thermal gratings arise from the relaxation of excited-state population gratings that are formed from the intensity modulation created by crossing two beams of identical frequency and polarization. When the two beams are cross polarized there are no intensity or population gratings and, consequently, no thermal gratings. For example, in the processes shown in Figs. 1(a), 2(a), and 3 the two PUMP beams (1 and 2) will form an excited-state population grating in the YYYY and YXYX configurations but not in the YYXX and YXXY configurations. Finally, the use of different polarization configurations in two-color RFWM provides the spectroscopist with another

mechanism to use in unraveling complex or congested spectra. For example, at low J the YYXX configuration for RFWM-SEP process (a) greatly enhances RR PUMP/DUMP combinations while YXXY enhances RP combinations. These types of rotational branch enhancements provide additional leverage in making rotational assignments in congested spectra.

6. ACKNOWLEDGMENTS

7. REFERENCES

1. R. L. Farrow and D. J. Rakestraw, Science **257**, 1894 (1992).
2. P. Ewart and S. V. O'Leary, Opt. Lett. **11**, 279 (1986).
3. T. Dreier and D. J. Rakestraw, Opt. Lett. **15**, 72 (1990); Appl. Phys. B **50**, 479 (1990).
4. S. Williams, R. N. Zare, and L. A. Rahn, J. Chem. Phys. **101**, 1093 (1994).
5. S. Williams, D. S. Green, S. Sethuraman, and R. N. Zare, J. Amer. Chem. Soc. **114**, 9122 (1992).
6. S. Williams, L. A. Rahn, P.H. Paul, J. W. Forsman, and R. N. Zare, Opt. Lett. **19**, 1 (1994).
7. T. G. Owano, C. H. Kruger, D. S. Green, S. Williams, and R. N. Zare, Diamond Relat. Mater. **2**, 661 (1993).
8. D. S. Green, T. G. Owano, S. Williams, D. G. Goodwin, R. N. Zare, and C. H. Kruger, Science **259**, 1726 (1993).
9. T. G. Owano, E. H. Wahl, C. H. Kruger, D. S. Green, and R. N. Zare, Proc. of the 11th Int. Symp. on Plasma Chemistry, 416 (1993).
10. Q. Zhang, S.A. Kandel, T.A.W. Wasserman, and P.H. Vaccaro, J. Chem. Phys. **96**, 1640 (1992).
11. P. H. Vaccaro, in *Molecular Dynamics and Spectroscopy by Stimulated Emission Pumping*, H.-L. Dai and R. W. Field, eds., *Advances in Physical Chemistry*, C.-Y. Ng, ed. (World Scientific Publishing, 1994).
12. E. F. McCormack, S. T. Pratt, P. M. Dehmer, and J. L. Dehmer, Chem. Phys. Lett. **211**, 147 (1993); Chem. Phys. Lett. **227**, 656 (1994).
13. M.A. Buntine, D.W. Chandler, and C.C. Hayden, J. Chem. Phys. **102**, 2718 (1995).
14. M.A. Buntine, D.W. Chandler, and C.C. Hayden, J. Chem. Phys. **97**, 707 (1992).
15. T. J. Butenhoff and E. A. Rohlfing, J. Chem. Phys. **97**, 1595 (1992).
16. H. J. Eichler, P. Gunter, and D. W. Pohl, *Laser-Induced Dynamic Gratings* (Springer-Verlag, Berlin, 1986).
17. T. J. Butenhoff and E. A. Rohlfing, J. Chem. Phys. **98**, 5460 (1993).
18. J. R. Dunlop and E. A. Rohlfing, J. Chem. Phys. **100**, 856 (1994).
19. T. J. Butenhoff and E. A. Rohlfing, J. Chem. Phys. **98**, 5469 (1993).
20. S. Williams, J. D. Tobiason, J. R. Dunlop, and E. A. Rohlfing, J. Chem. Phys. **102**, xxxx (1995).
21. S. Williams, R. N. Zare, and L. A. Rahn, J. Chem. Phys. **101**, 1072 (1994).
22. S. A. J. Druet, and J.-P. E. Taran, Prog. Quantum Electron. 7, 1 (1981).
23. Y. Prior, IEEE J. Quantum Electron. **QE-20**, 37 (1984).
24. T. K. Yee and T. K. Gustafson, Phys. Rev. A **18**, 1597 (1978).
25. R. Trebino, Phys. Rev. A **38**, 2921 (1988).
26. R. N. Zare, *Angular Momentum* (Wiley, New York, 1988).
27. E. A. Rohlfing and J. E. M. Goldsmith, J. Chem. Phys. **90**, 6804 (1989); J. Opt. Soc. Amer. B 7, 1915 (1990).
28. J. D. Tobiason, J. R. Dunlop, and E. A. Rohlfing, J. Chem. Phys., in press (1995).

DISCLAIMER